PCCP

PAPER

View Article Online
View Journal | View Issue

Cite this: *Phys. Chem. Chem. Phys.*, 2021, **23**, 15224

Structural and dynamic properties of some aqueous salt solutions†

Olivera Drecun,[a] Alberto Striolo *[a] and Cecilia Bernardini[b]

Received 10th October 2020,
Accepted 24th June 2021

DOI: 10.1039/d0cp05331g

rsc.li/pccp

Aqueous salt solutions are utilized and encountered in wide-ranging technological applications and natural settings. Towards improved understanding of the effect of salts on the dynamic properties of such systems, dilute aqueous salt solutions (up to 1 molar concentration) are investigated here, *via* experiments and molecular simulations. Four salts are considered: sodium chloride, for which published results are readily available for comparison, ammonium acetate, barium acetate and barium nitrate, for which published data are scarce. In the present work, molecular dynamics (MD) simulations are conducted to quantify viscosity and water self-diffusion coefficients, together with rheometry and Pulsed Field Gradient Spin Echo (PFGSE)-NMR experiments for validation. Simulation predictions are consistent with experimental observations in terms of trend and magnitude of salt-specific effects. Combining insights from the approaches considered, an interpretation of the results is proposed whereby the capacity of salts to influence bulk dynamics arises from their molecular interfacial area and strength of interaction with first hydration-shell water molecules. For the concentration range investigated, the interpretation could be useful in formulating aqueous systems for applications including the manufacturing of advanced catalysts.

Introduction

The structural and transport properties of aqueous salt solutions manifest from molecular structure and interactions, *i.e.* the substance itself, externally applied force (*e.g.* shear rate), and ambient conditions, namely temperature and pressure. Molecular structure and interaction mechanisms can be probed *via* theoretical, experimental and computational approaches. Among computational approaches, molecular dynamics (MD) simulations at atomistic resolution have been widely implemented to elucidate the mechanisms responsible for macroscale experimental observables.[1–5]

Of interest here are transport and structural properties of dilute aqueous salt solutions, and the influence of salt-specific effects. Salt-specific effects were first addressed by Hofmeister, whose series was conceived as a qualitative ranking of ions regarding their ability to solubilize or precipitate proteins in aqueous solution.[6] The concept has since been applied far beyond its original context. The resulting extent of series permutations and terminology[7] suggests the only unifying conclusion is that of no universal series capable of explaining all observed salt-specific effects.

In aqueous solutions, observed salt-specific effects have long been associated with the capacity of ions to 'make' ('kosmotropic') or 'break' ('chaotropic') water hydrogen-bonding structure, mainly within the first ion–water coordination shell. This relates to ion solvation entropy – entropy change of water molecules due to presence of an ion[8,9] – and the activation energy of disengaging a water molecule from the first coordination shell of an ion, compared to that of another water molecule.[10,11] Parsing contributions to solvation entropy due to the ion and due to water, 'kosmotropic' ions are mostly found to decrease the entropy of water molecules, with the opposite effect for 'chaotropic' ions. Experimental studies have since honed this interpretation,[12–16] suggesting that Hofmeister effects in aqueous solution are the result of direct ion–solvent interactions that give rise to extended hydration shells.[17,18]

Considering Hofmeister-type mechanisms in electrolyte solutions, colloids and protein systems, the comprehensive review of Salis and Ninham[19] suggests that any theory behind accurate modelling of Hofmeister effects requires the inclusion of dispersion forces, while also accounting for the chemical nature of interacting species. The latter has, at qualitative level, been implemented successfully by the law of matching water affinities (LMWA) to describe ion–ion and ion-charged surface site interactions.[20,21] The importance of dispersion forces has been emphasized in explaining the properties of biological and colloidal systems;[22] correlations between pH, the isoelectric point (pI) and the experimentally-observed reversed and direct

[a] *Department of Chemical Engineering, University College London, UK. E-mail: a.striolo@ucl.ac.uk*
[b] *Johnson Matthey Technology Centre, Blount's Ct, Sonning Common, Reading, UK*

† Electronic supplementary information (ESI) available. See DOI: 10.1039/d0cp05331g

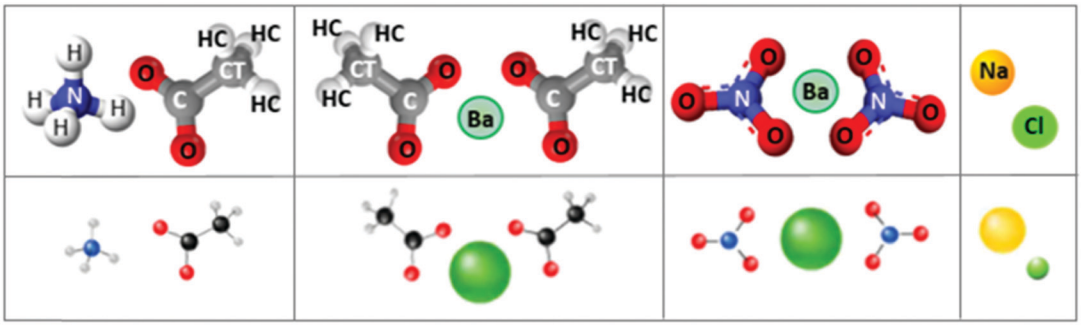

Fig. 1 Salt (ion-pair) schematics. Left to right: ammonium acetate, barium acetate, barium nitrate, sodium chloride. Top panel: ball and stick representation, with implemented atom notations. Lower panel: schematics indicate relative atomic sizes. Radii are taken from an empirical system of unified atomic-ionic radii, suitable for describing anion–cation contacts in ionic structures.[24–26]

Hofmeister sequences emerge from theory that incorporates the non-linear coupling of ionic dispersion and electrostatic forces.[23]

Aqueous solutions of ammonium acetate, barium acetate, barium nitrate and sodium chloride, ≤ 1 molar concentration, at ambient conditions, are the focus of this study (Fig. 1). Of these, the structural and dynamic properties of sodium chloride solutions are the most-documented by both MD simulations[27–34] and experiments.[35–37] Amongst its widespread occurrences, in geological settings, sodium chloride is the most common solute in aqueous fluids; its thermodynamic properties are therefore essential for modelling and interpreting many geological processes.[34] Ammonium acetate is commonly used as a solution buffer (at $\sim$pH 4.75 or 9.25)[38] and acidity regulator, among numerous other industrial applications.[39] Barium, incorporated as barium oxide within the washcoat layer of three-way catalytic converters, is an important trap and storage component for NO_2 in the Lean NOx Trap mechanism.[40] For this application, a precursor aqueous solution incorporating barium, nitrate and acetate ionic species is combined with a suspension of inorganic mixed oxides to impregnate the substrate; thermal decomposition to barium oxide occurs during subsequent calcination.

Despite diverse important applications, published data on the structural and dynamic properties of these aqueous salt solutions (apart from sodium chloride) are limited. In the present work, viscosity and self-diffusion coefficients are quantified using atomistic MD simulations to probe the ion-induced hydration structure and dynamics at molecular scale, together with rheometry and NMR experiments.

In what follows, new experimental and computational data are presented, testing simulation predictions for the properties of interest using existing force-field parameters. Results are correlated with physicochemical and thermodynamic properties of the corresponding ions, compiled from literature data, to identify the mechanisms through which the salts considered could modulate bulk transport properties of their aqueous solutions.

Simulation details

Methods

All simulations were performed using the freely available software LAMMPS,[41] (version 16 Mar 2018). The velocity Verlet algorithm[42] was implemented to integrate the equations of motion, with a 1 fs time step. Simulations were conducted with periodic boundary conditions in the canonical ensemble: constant number of particles (N), volume (V) and temperature (T), maintained by the Nosé–Hoover thermostat[43,44] (100 fs damping parameter). A cubic simulation box containing 11 089 water molecules was used, with side-length varied between 69.3–69.7 Å to attain experimental densities. Long-range interactions were treated with the particle–particle–particle–mesh (pppm) solver.[45]

Force-fields

After initial screening of three water models (Fig. S1 of ESI†), the SPC/E model[46] was utilized, based on yielding satisfactory agreement with experimental properties of interest, modest computational cost and broader compatibility compared to the TIP4P/2005[47] water model. In our simulations, O–H bond lengths and the H–O–H angle in each water molecule were maintained rigid using the SHAKE algorithm,[48] as implemented in LAMMPS.

Force fields parameters developed for use in conjunction with the SPC/E water model were applied to simulate ion pairs where possible. The widely used Joung–Cheatham model[49] for sodium and chloride ions, parameterized for SPC/E water, was therefore implemented, without polarizability. For barium nitrate, parameters for the nitrate ion[50] have previously been utilized to reproduce ion transport properties in aqueous (SPC/E) solutions of sodium and potassium, but not barium, nitrate. The parameters were implemented here with those of Mamatkulov *et al.*[51] for the barium ion, developed to reproduce the solvation free energy of divalent ions with SPC/E water. For ammonium acetate, a recently developed parameter set[52] incorporating the acetate ion, optimized to reproduce interactions with (TIP3P) water, and physiologically relevant cations, including ammonium, was utilized. The new parameterization improves upon limitations of the original GAFF[53–56] parameters, namely, the overestimation of anion–cation interactions, leading to an excessive number of contact ion pairs in solutions of carboxylate ions (such as acetate). Within the parameterisations implemented, ion pairs are free to associate or dissociate in response to system conditions. To quantify the dissociation behaviour, ion–ion radial distribution functions were computed (Fig. S2, ESI†). The results

suggest that NaCl is readily dissociated at the conditions considered, while the other ion pairs show different dissociation tendencies, qualitatively consistent with physicochemical properties of these systems.

Force field parameters as implemented in this work are presented in Table S1 of the ESI.† Interaction energies are modelled using the Lennard-Jones and Coulomb potentials. Non-bonded interactions are truncated at 10 Å, with the exception of aqueous sodium chloride simulations, for which non-bonded interactions are truncated at 9 Å. Mixed atom-type interaction potentials are calculated from self-interaction parameters using Lorentz–Berthelot combining rules.

Algorithms

Viscosity. Shear viscosity at 299.15 K (26 °C) was obtained from non-equilibrium molecular dynamics (NEMD) simulations implementing non-Hamiltonian SLLOD equations of motion,[57–59] whereby Couette flow is imposed *via* continuous deformation of a periodic simulation box, changing the tilt factor (initially zero; orthogonal) at a constant strain rate. In this algorithm, for each atom, a position-dependent streaming velocity induced by the changing simulation box shape is subtracted from the actual velocity to obtain the thermal velocity, used in the temperature computation.

Viscosity values are obtained from three independent 12 ns simulations per concentration, for each salt type. The first 6 ns are dropped from analysis, with the remaining 6 ns used for production. Viscosity values, computed every 500 fs, are averaged over the latter 6 ns to yield a mean value for each simulation production run. Simulation viscosity values quoted in the manuscript are the mean average of three production runs. Viscosity results for pure water, inclusive of block averages and error analysis, are reported in Table S2, ESI,† as a function of simulation time. This analysis was used to establish the simulation time required to achieve reliable data (Tables S3 and S4, ESI†). The reported uncertainty in our viscosity calculations is defined as standard deviation from the mean average value of the three production runs, and lies within 2%, for all salt types and concentrations considered.

Diffusion coefficients and radial distribution functions. Equilibrium MD simulations were conducted at 299.15 K (26 °C) to obtain diffusion coefficients for both ions and water, and to compute radial distribution functions (RDFs). Simulations were conducted for 4.5 ns, of which the first 1 ns was used for equilibration; the remaining 3.5 ns for production. RDFs and mean-square displacements (MSD) were computed using LAMMPS source code.

Self-diffusion coefficients (D) were obtained from the slope of MSD-over-time plots using the Einstein relation[60,61] with n (dimensionality of the diffusion process) = 3:

$$\lim_{t\to\infty} \mathrm{MSD}(t) = 2nD \quad (1)$$

The uncertainty was calculated as standard deviation from the averages of three independent simulations per concentration, for each salt type (example shown in Table S5, ESI†).

Experimental methods

Shear (dynamic) viscosity

Aqueous salt solutions were prepared by volume, using 50 ml volumetric flasks (accuracy ±0.5 ml). Salts were weighed out using a Kern ABT analytical balance; resolution ±0.1 mg. Accuracy of concentration values for the prepared solutions is ≤1.32% (percentage difference) from the target concentrations (see ESI† excel file). For barium nitrate, the maximum concentration prepared was 0.3 M due to its low water solubility at ambient conditions.[62–64] It should be noted that ammonium and acetate ions in aqueous solution can undergo hydrolysis to ammonia and acetic acid, respectively; the extent of conversion depending on water pH [H^+]. Barium, sodium, nitrate and chloride ions are insensitive to pH. However, these effects are not considered in the discussion of the results reported, nor the simulations conducted and presented herein.

Viscosity measurements were conducted at 26 °C, using an Anton Paar modular compact rheometer (MCR 302) with Peltier plate temperature control and cone–plate geometry. Prior to measurements, samples were given 2 minutes to thermally equilibrate with the sample plate. Measurements were taken over a 60 second duration, with sampling interval of 1 s per

Table 1 Experimental component details for viscosity measurements

Experimental component:	Details	
Rheometer set-up:	RheoCompass™ pre-defined moving profile:	'Low viscosity'
Cone-and -plate geometry:	Measuring cone CP50-1	
	Diameter:	50 mm
	Angle:	1°
	Gap:	0.099 mm
Salts		
• Ammonium acetate	Certified AR for Analysis; Fisher Chemical	
• Barium acetate	99+%, Fisher Chemical	
• Barium nitrate	99+%, Fisher Chemical	
• Sodium chloride	99.9% BP, ACS, PH EUR, FCC; APC Pure	
Water	PURELAB Chorus 2+ Reference Water Purification System, inorganics resistivity (25 °C): >15 MΩ cm. Particle filtration: 0.2 μm	

data point, at a fixed shear rate of 300 s^{-1}. The results reported are the average of three measurements per solution, with a new sample loaded for each measurement. Further experimental details are provided in Table 1.

Translational self-diffusion

Self-diffusion measurements were conducted using a Magritek Spinsolve 60 Benchtop NMR spectrometer (60 MHz field strength). The Pulsed Field Gradient Spin Echo (PFGSE) technique, utilising ^{1}H (proton) nucleus spin diffusion, was implemented. With this technique, the dephasing of nuclear spins and attenuation of the magnetic resonance signal, a combined result of translational diffusion and the insertion of spatially defined gradient pulses, is used to measure molecular motion.

Spin echo[65] is generated by two successive radiofrequency (RF) pulses, typically a 90° (excitation)–180° (refocusing) pair of the same signal intensity and duration. The second pulse refocuses ('echoes') the magnetization of spins that have de-phased. However, molecular diffusion in the interval between gradient pulses means the refocusing will not restore the original spins entirely, causing attenuation of the NMR signal. The signal loss is directly dependent on the gradient pulse amplitude and duration. Signal decay due to diffusion, for constant gradient wave forms and in the case of Gaussian diffusion, is given by the Stejskal–Tanner[66] equation:

$$\ln(I_G/I_0) = -\gamma^2 G^2 \delta^2 (\Delta - \delta/3) D \quad (2)$$

In eqn (2), I_G and I_0 represent signal intensities in the presence and absence of the gradient pulses, respectively; γ is the gyromagnetic ratio and G is the gradient amplitude. Time between gradient pulses and pulse duration are represented by Δ and δ, respectively; these are user-set parameters. The $(\Delta - \delta/3)$ term is the diffusion time; the diffusion-coefficient is D. Parameters Δ and δ were set to 30 ms and 5 ms, respectively; a calibration value of 2.57×10^{-9} m^2 s^{-1} for water self-diffusion was obtained. User-defined temperature control within the measuring compartment was not possible with the NMR instrument used herein. However, the calibration value obtained suggests temperature conditions within the compartment between 26–29 °C, according to reference data.[67] The temperature recorded within the sample tube using a thermocouple, directly after NMR measurements were completed, was 26 °C. The combined influence of the user-set parameters and temperature control on the calibration value should be considered; addressing the latter, all samples were left to thermally equilibrate in the measuring chamber for 10 minutes prior to measurements, for internal consistency. Although temperature uncertainty is greater than desired, we consider the procedure implemented sufficient for the objective of achieving relative, rather than absolute, comparison of trends regarding salt-specific effects on transport properties in aqueous solutions. The results reported correspond to the average of three measurements per sample.

Results

To facilitate comparison between simulations and experiments, the results are expressed as the ratios η/η_0 and D/D_0, for viscosity and self-diffusion, respectively; reference values η_0 and D_0 are for pure water at 26 °C, atmospheric pressure. Regarding simulations, system size dependence of water self-diffusion values, for N = 128 to 2048 water molecules, was noted by Yeh and Hummer,[68] whereby larger systems produce higher D values. The ratio D/D_0, however, is independent of system size.[69] In what follows, results are presented both tabulated and graphed, to aid interpretation.

Normalized simulation and experimental viscosity data are shown in Table 2 and Fig. 2. For simulation results, standard deviations are $\leq$0.68% (as a percentage of the mean viscosity value, from three simulations per salt solution). For the experimental data, standard deviations are within 2.13% of the mean viscosity value as obtained from three measurements per salt solution. Error bars for all normalized data points are plotted in Fig. 2, but are not clearly visible because they are of the magnitude of the data-markers on the graphs. Results for aqueous sodium chloride solutions are within 1.98% of corresponding literature values[35] available at 25 °C from the comprehensive compilation of Ozbek *et al.*[35] These are consistent with values found across more recent publications[70,71] (a table conveniently summarizing experimental studies of the dynamic viscosity of aqueous sodium chloride solutions can be found in Aleksandrov *et al.*[72]), and data referenced by NIST.[73] The data of Ozbek *et al.*[35] is normalized and presented alongside the results of Fig. 2.

Normalized results for water self-diffusion coefficients at 26 °C are shown in Table 3 and Fig. 3. The statistical range of triplicate simulation results is of magnitude comparable to that of the plot data-markers. Standard deviation for simulation results is within 2% of the mean value, and $\leq$1.07% for mean values of experimental self-diffusion measurements, taken over three measurements per sample. Simulation results for NaCl solutions in Fig. 3 are shown together with (normalized) values from Fuentes-Azcatl *et al.*,[74] at 24.85 °C, utilising the same water model and ion parameters. Experimental data are

Table 2 Viscosity (η/η_0): comparison between simulation (Sim.) and experimental (Exp.) results. η_0 *i.e.* viscosity of pure water, mPa s: 0.6882 (simulation), 0.8567 (experimental), at 26 °C. Molar concentrations for barium nitrate, where different, are shown in parentheses (*)

	Ammonium acetate		Barium acetate		Barium nitrate		Sodium chloride	
Molar concentration	Sim.	Exp.	Sim.	Exp.	Sim.	Exp.	Sim.	Exp.
0.1	1.0245	1.0807	1.0829	1.1269	1.0491	1.0703	1.0203	1.0600
0.5 (*0.2)	1.1431	1.1717	1.5213	1.4883	1.1034	1.0936	1.1226	1.0947
1.0 (*0.3)	1.3252	1.2961	2.1977	2.1103	1.1979	1.1183	1.2577	1.1617

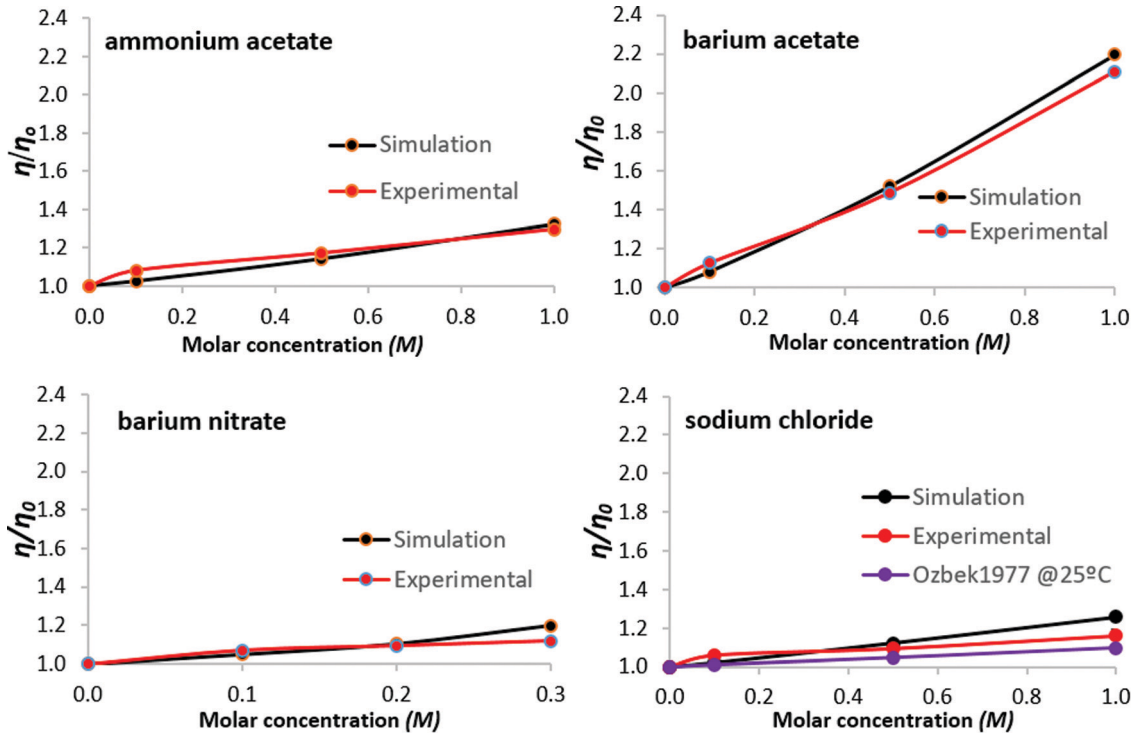

Fig. 2 Viscosity of aqueous salt solutions at 26 °C: salt concentration dependence. Experimental data from Ozbek *et al.*,[35] for aqueous sodium chloride at 25 °C, are normalized and included for comparison. Lines are guides to the eye.

Table 3 Self-diffusion (D/D_0): comparison between simulation (Sim.) and experimental (Exp.) results. Self-diffusion coefficient of pure water (D_0), 10^{-9} m^2 s^{-1}: 2.77 (simulation), 2.57 (experimental), at 26 °C. Molar concentrations for barium nitrate, where different, are shown in parentheses (*)

	Ammonium acetate		Barium acetate		Barium nitrate		Sodium chloride	
Molar concentration	Sim.	Exp.	Sim.	Exp.	Sim.	Exp.	Sim.	Exp.
0.1	1.0072	0.9728	0.9386	0.9058	0.9856	0.9883	0.9964	1.0000
0.5 (*0.3)	0.9170	0.9105	0.7473	0.7354	0.8664	0.9221	0.8917	0.9650
1.0	0.8087	0.8366	0.5560	0.5689			0.8375	0.9377

sourced from McCall & Douglass,[75] who conducted experiments at 23 °C using the proton magnetic resonance spin-echo method.

Fig. 4 presents ion–water RDFs obtained for the salt solutions at 1 M concentration, grouped to aid comparison. Results for all salt concentrations, with comparison of fit to nearest available literature data, are provided in ESI,† Fig. S3–S6 for ammonium acetate, barium acetate, sodium chloride and barium nitrate, respectively.

Discussion

While discrepancies between simulation predictions and experimental results persist in absolute terms, the magnitude of relative change predicted for viscosity and self-diffusion coefficients, as shown by the normalized results of Fig. 2 and 3, is in good agreement.

For viscosity, simulation results lie within 8.3% of experimental values; for self-diffusion this extends to 12%, notably for sodium chloride. For all solutions considered, viscosity increases with salt concentration, with proportionally opposite self-diffusion coefficient trends. Regarding self-diffusion coefficient predictions from MD simulations, Kim *et al.* (2012)[69] observed that all commonly used water models (including SPC/E), simulated with a selection of 'structure-making' and 'structure-breaking' salts, predict a decrease of D as salt concentration increases, even for salts that experimentally yield increased values. This was attributed to the form of the interaction potentials for water models, *i.e.*, the use of simple point charge models to treat water hydrogen bonding and the Lennard-Jones potential to treat non-bonded van der Waals interactions. In the present work, the agreement with experimental trends suggests that salt-specific effects on dynamics are reasonably reproduced by our simulations, though it is recognised that all the salts considered here decrease water self-diffusion, as measured experimentally.

Both simulation and experimental results presented here show barium acetate as having the greatest effect on increasing viscosity and simultaneously reducing the mobility of water molecules, as

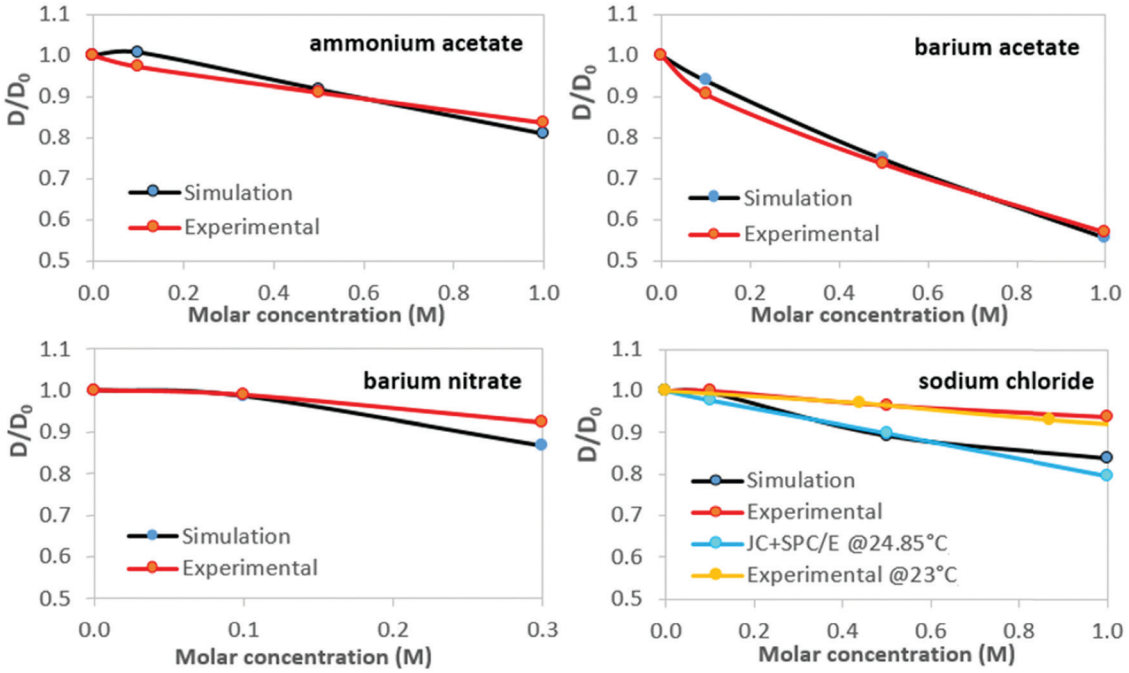

Fig. 3 Water self-diffusion in aqueous salt solutions at 26 °C: concentration dependence. Clockwise, from top left: ammonium acetate, barium acetate, sodium chloride, barium nitrate. Water self-diffusion reference data for aqueous sodium chloride solutions (MD simulation[74] and experimental[75]) are shown for comparison. Lines are guides to the eye.

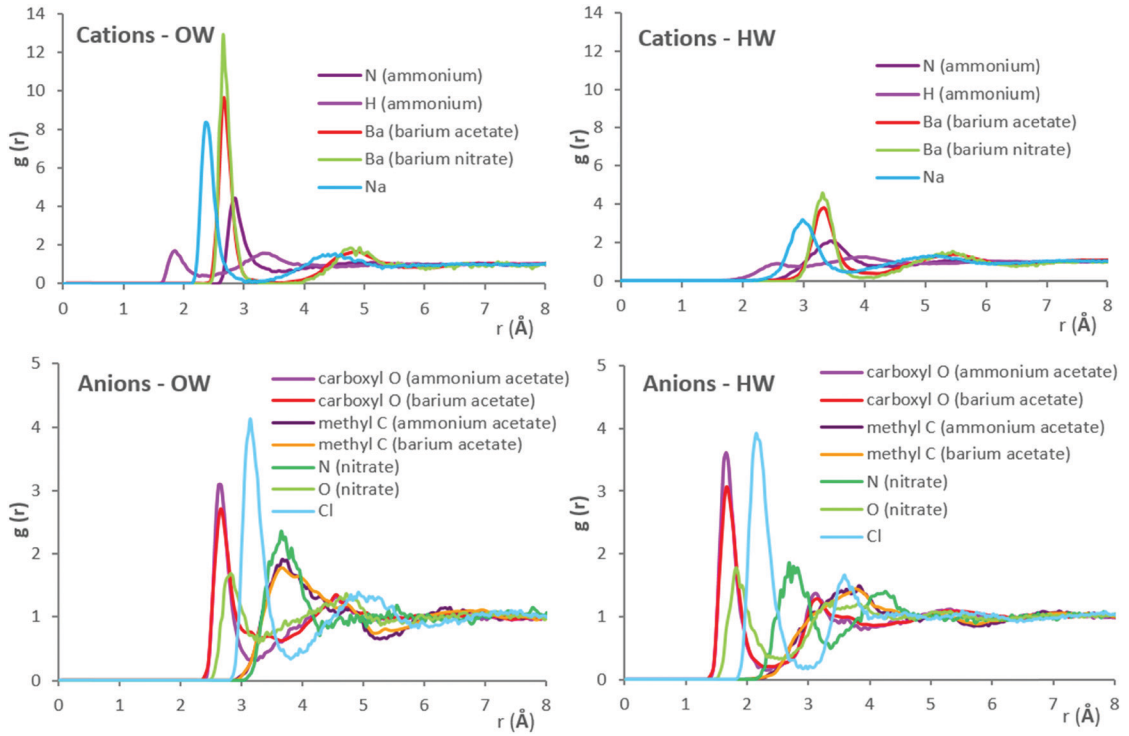

Fig. 4 Ion–water (OW, HW) radial distribution functions (RDFs) obtained from MD simulations for salt solutions at 1 M concentration, except barium nitrate (0.3 M, which is near its solubility limit at 26 °C).

indicated by the decreased self-diffusion coefficients. Sodium chloride produces the weakest effects, with ammonium acetate and barium nitrate in between, although analysis for barium nitrate is restricted by its low solubility limit.

RDF results are generally in good agreement with literature data, as shown in Fig. S3–S6 of ESI.† Fig. S3 (ESI†) shows results from Monte-Carlo (MC) molecular simulations with TIP4P water for both acetate and ammonium ions[76] and classical MD simulations with SPC/E for the acetate ion.[77] Results of the present work for the acetate ion are near-identical to literature simulation data, while slight discrepancies emerge for ammonium. For the latter, comparison with *ab initio* simulation data[78] indicate an over-prediction of first-shell number densities by MC and MD methods, for interactions with oxygen atoms of water (OW) in particular. For barium–water systems, available literature data from experiment[51] and classical MD simulations[51] with SPC/E locate the Ba–OW maxima at 2.75 Å and 2.69 Å, respectively. Using the same water model and barium ion parameters yields the corresponding maxima at 2.65 Å, in the presence of acetate counter-ions. Ion–water RDFs obtained here for sodium chloride appear indistinguishable from classical MD simulation data from literature (at 24.85 °C, $M = 1.3877$),[79] which were also obtained using SPC/E and Joung–Cheatham ion parameters (see Fig. S5, ESI†). However, compared to results obtained from the Empirical Structural Refinement (EPSR) approach,[79] over-structured first solvation shells predicted by classical MD simulations become apparent. For barium nitrate systems, the OW number-density peaks at 3.65 Å from the nitrate anion (nitrogen), which agrees with experimental values of 3.5 ± 0.311 Å.[81] Results are in reasonable agreement with literature data shown for the nitrate ion in Fig. S6 (ESI†), sourced from an MD study of rotational dynamics in aqueous (SPC/E) nitrate solutions,[80] albeit for a dilute system (0.102 M) of potassium nitrate at 26.85 °C.

Considering the RDFs of Fig. 4, out of the cations, barium possesses the most radially distant first hydration shell with highest number density of both (water) oxygens and hydrogens; out to ~3 and 4 Å, respectively. RDFs of Ba–OW, Ba–HW for barium nitrate and barium acetate are virtually identical in terms of peak positions. This suggests that the anion has no significant effect on hydration shell spacing around the cation. The greater height of the first Ba–OW peak in the presence of the nitrate ($g_{(Ba–OW)} \sim 13$) compared to the acetate anion ($g_{(Ba–OW)} \sim 10$) is possibly due partly to the lower concentration of barium nitrate (0.3 M, due to solubility limits) and to the corresponding decreased 'competition' for water binding sites. Considering the anions, in the presence of barium, water (OW) structuring around (acetate) methyl carbon is diffuse compared to (nitrate) nitrogen; out to ~5 Å, compared to ~4.25 Å. The diffuse hydration shells suggest a greater orientational freedom of the inhabitant water molecules. Additionally, acetate (carboxylate) oxygens appear more neutral to OW when compared to nitrate oxygens; $g_{(O–OW)} \sim 2.75$ and 1.75, respectively. Three nitrate oxygens (H-bond acceptors) contrast with the acetate possessing two, together with a hydrophobic CH_3 group. Considering the above, the greater number density of OW around barium in barium nitrate, compared to barium acetate aqueous solution, could be therefore partly interpreted as an effect of lesser 'OW interaction engagement' from its (nitrate) anion counterpart.

For the ammonium cation, the higher peaks, at closer proximity, for OW compared to HW around both the nitrogen and hydrogen atoms, implicate first-shell water molecules as H-bond acceptors for ammonium hydrogens. Comparing RDFs for ammonium acetate and barium acetate (at 1 M concentration), water structuring around acetate (methyl) carbon appears scarcely affected by the cation (whether monovalent ammonium or divalent barium). Considering the oxygen (carboxylate) atoms of acetate however, the occurrence of OW in the transition between first and second hydration shells in the presence of ammonium shows a deeper minima (at 3.1 Å), compared to barium. With the prior comparison of anion effects between barium nitrate and barium acetate, it would appear, at least for the salts presented here, that water-structuring effects of an ion can be affected by its counter-ion; such mutual effects are relevant to phenomena across varied contexts, including water structuring,[82] behaviours of ionic liquids[83,84] and battery performance energetics.[85] For ion hydration shell population densities, it appears that OW around cations comprises the biggest share, especially for the large monoatomic cations. A significantly greater contrast between OW and HW population densities around cations, than for anions, is also apparent, as shown by the RDF peak heights.

To explain the contrasting influences on viscosity and water self-diffusion between sodium chloride and barium acetate, an interplay of factors becomes evident when considering the RDFs, and visualising the ion combinations as in Fig. 1. The RDFs show sodium as the second-most water-structuring cation after barium, due to its smaller size; both are monoatomic, with similar charge density. The weakness of sodium chloride therefore appears to stem from the chloride anion; furthest-placed first hydration shell, weakly bound, due to its large radius and low charge density. The populous, narrow first hydration shell of divalent barium is the combined effect of its large surface area with high charge density. For the acetate counter-ion, observations include diffuse hydration shells around a complex spatial arrangement of charges and resulting attraction–repulsion configurations, compounded by the doubled anion concentration in solution needed to attain charge neutrality. Both variants of interaction strength and engagement, together, appear to strongly affect the bulk dynamics. In water-structuring terms, barium could be described as kosmotropic, as it promotes narrow, densely-populated hydration shells. Conversely, the greater orientational freedom of diffusely bound water molecules around the acetate, with its hydrophobic (methyl group) and hydrophilic (carboxylate) 'ends', yields a chaotropic effect (for approximate viscosity Jones–Dole coefficients obtained from our experimental data, see ESI,† Fig. S7). For the acetate anion, a greater 'local drag' experienced by bulk water moving past interfacial waters could be anticipated. For polyatomic ions, MD simulations have shown that the translational and rotational motions of ions are coupled; to which the dynamics of surrounding water molecules are coupled in turn.[86] Furthermore, for the ions investigated, which included nitrate and acetate, the extent of geometric asymmetry was found to influence diffusivity. Nitrate undergoes faster

Table 4 Ion properties, at ambient conditions, sourced from literature

	Barium	Ammonium	Sodium	Nitrate	Acetate	Chloride
Aqueous ionic radii,[87] Å	1.36	1.48	1.02	1.79	1.62	1.81
Experimental molar Gibbs energy of hydration ($\Delta_{hyd}G$/kJ mol^{-1})[87]	−1250	−285	−365	−300	−365	−340
Ion–water coordination number	8[88]	4–5[89]	5[90]	21[91]	∼16[92]	∼6[93]
					CH_3 ∼ 10, COO ∼ 5.5–6.5	
Topological polar surface area,[94] Å^2	0	1	0	62.9	40.1	0
'Complexity'[94,96]	0	0	0	18.8	25.5	0
Enthalpy of formation (kJ mol^{-1})[95]	−537.6	−132.5	−240.1	−207.4	−486.0	−167.2
Gibbs free energy of formation (kJ mol^{-1})[95]	−560.8	−79.3	−261.9	−111.3	−369.3	−131.2
Standard entropy (J mol^{-1} K^{-1})[95]	9.6	113.4	59.0	146.4	86.6	56.5

rotational jump motion in water, with enhanced diffusivity, compared to acetate; rotational diffusivity values obtained were 0.056 ± 0.0024 ps^{-1} and 0.02 ± 0.003 ps^{-1}, respectively.[86] Rotational dielectric friction of the aqueous nitrate ion, 1.44 × 10^{-24} erg s^{-1}, compared to 1.57 × 10^{-24} erg s^{-1} for acetate,[86] confirms the contribution of charge distribution complexity, as well as geometric asymmetry, to hindrance of rotational motion in water.

For further interpretation of our results, selected physico-chemical data for the ions considered are compiled in Table 4. In light of the over-structuring of all commonly utilised water models for OW–HW interactions (Fig. S1, ESI†) and possible effects on ion–water coordination number predictions, the coordination numbers in Table 4 are sourced from experimental and quantum-level simulation data.

The aqueous ionic radii[87] are calculated as the average distance between the ion and its nearest water molecules, obtained from diffraction experiments and simulations. Topological polar surface area[94] is defined as the surface sum over all polar atoms in a molecule. The rating for 'complexity' is computed using the Bertz/Hendrickson/Ihlenfeldt formula,[96] and provides a rough estimate in terms of the displayed structural features, including symmetry, and the elements contained. Similar formulations, incorporating volume, bulkiness and surface area parameters have been implemented since for calculating thermodynamic properties of 1:1 aqueous salt solutions.[97]

Also incorporated in Table 4 are values for enthalpy of formation, Gibbs energy of formation and standard entropy of the aqueous ions.[95] Data refer to 'standard state', *i.e.* the hypothetical ideal solution with molality M = 1 mol kg^{-1} (mean ionic molality, in the case of a species assumed to dissociate at infinite dilution), at 25 °C and 1 atm. For the case of both barium and acetate ions, breaking of water–ion interactions appears energetically unfavourable. For nitrate, the correlation of polar surface area and entropy suggests polarizability as another strong influencing mechanism on water ordering and interaction strength, in polar solutes. Similar influences have been proposed to explain a weaker influence of cations compared to anions on water-ordering, due to the larger positive electrostatic potential 'visible' to anions at the water molecule surface.[98]

The direct effect of ions on water structure, as observed from the RDFs, appears spatially limited to a radial zone of 8 Å from the ion–water interface. If so, a question arises as to whether bulk transport properties observed at macroscopic scale are simply a multiplication, across orders of magnitude, of molecular-scale phenomena, or if cumulative indirect effects emerge which may also be part of the picture. To this end, approximating the proportion of total water of the system 'engaged' in the first hydration shell of ions, and perhaps considering the resulting network through which remaining 'un-bound' waters flow, may be helpful. Using the coordination numbers of Table 4, it can be estimated that, in aqueous solutions of 1 molar concentration, ∼20% of total water molecules are 'engaged' with sodium chloride in first hydration shells; this value increases to ∼72% of total water molecules for barium acetate (details in Table S6, ESI†). These estimates suggest that the salt-specific effects on macroscopic dynamics observed in Fig. 2 and 3, for the most part, might arise cumulatively from the direct effect of the ions on their hydration shells. In this way, ions with hydration shells containing more water molecules could exert stronger influence on bulk dynamics (whether accelerating or decelerating), depending on charge distribution and ion–water interaction strengths.

Conclusions

Bulk dynamics for the aqueous solutions of four 1:1 and 2:1 salt types have been investigated utilising experiments and classical molecular dynamics (MD) simulations. Results for aqueous sodium chloride are in good agreement with published data. New data are reported for viscosity and water self-diffusion coefficients for aqueous solutions of ammonium acetate,[99] barium nitrate[100] and barium acetate[101] salts, for which scarce data were available in the open literature.

Our results show that atomistic MD simulations, with the force-field combinations applied here, are able to predict results for the properties of interest which, when normalized, closely agree with experimental trends.

The availability of macroscopic experimental data, together with atomistic details from MD simulations, facilitates a discussion of the results that addresses the synergy of various ion attributes, analysed above in the context of published data to achieve a 'holistic' interpretation. Influencing mechanisms, when considering salt-specific effects and macroscopic transport properties of the aqueous solutions, are found to be ion size and charge density (for monoatomic ions), but also size and number of component atoms (for multi-atomic ions), their spatial arrangement, polarizability and radial accessibility

(*i.e.*, 'visibility' of component atoms to surrounding water molecules at the interface). All these factors are found to be interlinked with interaction strength and energetics. In yielding the energetically strong interactions that characterize the 'strongest salts' of the present work (in terms of slowing water dynamics), polar surface area, charge density and charge distribution complexity emerged as significant ion attributes.

The findings presented could be useful in interpreting experimental results for other aqueous salt solutions and for formulating aqueous systems within the development of many industrial applications, including the production of catalytic converters.

Conflicts of interest

There are no conflicts to declare.

Acknowledgements

This project was supported financially by Johnson Matthey and, in part, by the UCL Department of Chemical Engineering. We are grateful to Dr Andy York at Johnson Matthey Technology Centre (Sonning Common), for guidance with the experimental setup of PFGSE-NMR water self-diffusion measurements, and to Dr Misbah Sarwar, for comments on this manuscript. Within the UCL Chemical Engineering Department, we owe special thanks to Prof. Panagiota Angeli for accommodating time on the rheometer, and to Dr Simona Migliozzi, for her guidance with viscosity measurements. Computational time and resources were provided by University College London Research Computing Platforms Support (Myriad cluster). We thank Dr Anh T. V. Phan for her support in the set-up of MD simulations. We are also grateful to Prof. Pierandrea Lo Nostro and Dr Robin Curtis, for discussions on salt-specific effects within the Hofmeister framework.

References

1 G. C. Sosso, T. Li, D. Donadio, G. A. Tribello and A. Michaelides, Microscopic Mechanism and Kinetics of Ice Formation at Complex Interfaces: Zooming in on Kaolinite, *J. Phys. Chem. Lett.*, 2016, **7**(13), 2350–2355.

2 M. Fitzner, G. C. Sosso, S. J. Cox and A. Michaelides, Ice is born in low-mobility regions of supercooled liquid water, *Proc. Natl. Acad. Sci. U. S. A.*, 2019, **116**(6), 2009–2014.

3 S. Chatterjee, P. G. Debenedetti, F. H. Stillinger and R. M. Lynden-Bell, A computational investigation of thermodynamics, structure, dynamics and solvation behavior in modified water models, *J. Chem. Phys.*, 2008, **128**, 124511.

4 Z. Yan, S. V. Buldyrev, P. Kumar, N. Giovambattista, P. G. Debenedetti and H. E. Stanley, Structure of the first- and second-neighbor shells of simulated water: Quantitative relation to translational and orientational order, *Phys. Rev. E: Stat., Nonlinear, Soft Matter Phys.*, 2007, **76**, 051201.

5 J. D. Durrant and J. A. McCammon, Molecular dynamics simulations and drug discovery, *BMC Biol.*, 2011, **9**, 71.

6 W. Kunz, J. Henle and B. W. Ninham, Zur Lehre von der Wirkung der Salze' (about the science of the effect of salts): Franz Hofmeister's historical papers, *Curr. Opin. Colloid Interface Sci.*, 2004, **9**(1–2), 19–37, DOI: 10.1016/j.cocis.2004.05.005.

7 D. Roberts, J. Warwicker and R. Curtis, Chapter 7: Molecular Modeling for Protein Aggregation and Formulation, in *Computational Pharmaceutics: Application of Molecular Modeling in Drug Delivery*, ed. D. Ouyang and S. C. Smith, John Wiley & Sons, Ltd., 2015, Section 7.3.1, p. 129. Available at: https://onlinelibrary.wiley.com/doi/pdf/10.1002/9781118573983.

8 B. Hribar, N. T. Southall, V. Vlachy and K. A. Dill, How ions affect the structure of water, *J. Am. Chem. Soc.*, 2002, **124**, 12302–12311.

9 G. A. Krestov, *Thermodynamics of solvation*, Ellis Horwood, New York, 1990.

10 O. Y. Samoilov, A new approach to the study of hydration of ions in aqueous solutions, *Discuss. Faraday Soc.*, 1957, **24**, 141–146.

11 O. Y. Samoilov, in *Water and Aqueous Solution: Structure, Thermodynamics and Transport Processes*, ed. R. A. Horne, Wiley-Interscience, New York, 1972, pp. 597–612.

12 A. W. Omta, M. F. Kropman, S. Woutersen and H. J. Bakker, Negligible Effect of Ions on the Hydrogen-Bond Structure in Liquid Water, *Science*, 2003, **301**, 347–349.

13 J. D. Batchelor, A. Olteanu, A. Tripathy and G. J. Pielak, Impact of Protein Denaturants and Stabilizers on Water Structure, *J. Am. Chem. Soc.*, 2004, **126**, 1958–1961.

14 Y. Marcus, Effect of Ions on the Structure of Water: Structure Making and Breaking, *Chem. Rev.*, 2009, **109**, 1346–1370.

15 Y. Marcus, Effect of Ions on the Structure of Water, *Pure Appl. Chem.*, 2010, **82**, 1889–1899.

16 P. Ball and J. E. Hallsworth, Water Structure and Chaotropicity: Their Uses, Abuses and Biological Implications, *Phys. Chem. Chem. Phys.*, 2015, **17**, 8297–8305.

17 M. T. Record, E. Guinn, L. Pegram and M. Capp, Faraday Discussion 160 Introductory Lecture: Interpreting and Predicting Hofmeister Salt Ion and Solute Effects on Biopolymer and Model Processes Using the Solute Partitioning Model, *Faraday Discuss.*, 2013, **160**, 9–44.

18 M. Andreev, J. J. de Pablo, A. Chremos and J. F. Douglas, Influence of Ion Solvation on the Properties of Electrolyte Solutions, *J. Phys. Chem. B*, 2018, **122**(14), 4029–4034.

19 A. Salis and B. W. Ninham, Models and mechanisms of Hofmeister effects in electrolyte solutions, and colloid and protein systems revisited, *Chem. Soc. Rev.*, 2014, **43**, 7358–7377, DOI: 10.1039/C4CS00144C.

20 K. D. Collins, Charge density-dependent strength of hydration and biological structure, *Biophys. J.*, 1997, **72**(1), 65–76, DOI: 10.1016/S0006-3495(97)78647-8.

21 K. D. Collins, Ions from the Hofmeister series and osmolytes: effects on proteins in solution and in the

crystallization process, *Methods*, 2004, **34**(3), 300–311, DOI: 10.1016/j.ymeth.2004.03.021.

22 L. A. Moreira, M. Boström, B. W. Ninham, E. C. Biscaia and F. W. Tavares, Hofmeister effects: Why protein charge, pH titration and protein precipitation depend on the choice of background salt solution, *Colloids Surf., A*, 2006, **282–283**, 457–463, DOI: 10.1016/j.colsurfa.2005.11.021.

23 M. Boström, F. W. Tavares, S. Finet, F. Skouri-Panet, A. Tardieu and B. W. Ninham, Why forces between proteins follow different Hofmeister series for pH above and below pI, *Biophys. Chem.*, 2005, **117**(3), 217–224.

24 CrystalMaker webpage: 'Elements, Atomic Radii and the Periodic Table', and refs therein. URL: http://crystalmaker.com/support/tutorials/atomic-radii/index.html [Accessed: 3rd May 2020].

25 CrystalMaker Element Tables: 'CPK Atomic-Ionic Radii', and refs therein. http://crystalmaker.com/support/tutorials/atomic-radii/resources/CPK_Atomic_Ionic_Radii.jpg.

26 J. C. Slater, Atomic Radii in Crystals, *J. Chem. Phys.*, 1964, **41**(10), 3199–3204, DOI: 10.1063/1.1725697.

27 S. Yue and A. Z. Panagiotopoulos, Dynamic properties of aqueous electrolyte solutions from non-polarisable, polarisable, and scaled-charge models, *Mol. Phys.*, 2019, 1–12.

28 A. L. Benavides and M. A. Portillo, *et al.*, A potential model for sodium chloride solutions based on the TIP4P/2005 water model, *J. Chem. Phys.*, 2017, **147**, 104501.

29 R. Fuentes-Azcatl and M. C. Barbosa, Sodium chloride, NaCl/ε: New Force Field, *J. Phys. Chem. B*, 2016, **120**, 2460–2470.

30 A. P. Lyubartsev and A. Laaksonen, Concentration effects in aqueous NaCl solutions. A Molecular Dynamics Simulation, *J. Phys. Chem.*, 1996, **100**(40), 16410–16418.

31 S.-B. Zhu and G. W. Robinson, Molecular-dynamics computer simulation of an aqueous NaCl solution: structure, *J. Chem. Phys.*, 1992, **97**, 4336.

32 M. Patra and M. Karttunen, Systematic comparison of force fields for microscopic simulations of NaCl in aqueous solutions: Diffusion, free energy of hydration, and structural properties, *J. Comput. Chem.*, 2004, **25**, 678–689.

33 H. Uchida and M. Matsuoka, Molecular dynamics simulation of solution structure and dynamics of aqueous sodium chloride solutions from dilute to supersaturated concentration, *Fluid Phase Equilib.*, 2004, **219**(1), 49–54.

34 J. P. Brodholt, Molecular dynamics simulations of aqueous NaCl solutions at high pressures and temperatures, *Chem. Geol.*, 1998, **151**(1–4), 11–19.

35 H. Ozbek, J. A. Fair and S. L. Phillips, *Viscosity of aqueous sodium chloride solutions from 0–150 °C*, Lawrence Berkeley National Laboratory, 1977. https://escholarship.org/uc/item/3jp6n2bf#main [Accessed: 25th February 2021].

36 S. L. Phillips, H. Ozbek, *et al.*, *Viscosity of NaCl and other solutions up to 350 °C and 50 MPa pressures*, Lawrence Berkeley National Laboratory, 1980. https://www.osti.gov/servlets/purl/6731414/ [Accessed: 25th February 2021].

37 J. Kestin, H. E. Khalifa and R. J. Correia, Tables of the dynamic and kinematic viscosity of aqueous NaCl solutions in the temperature range 20-150 °C and the pressure range 0.1-35 MPa, *J. Phys. Chem. Ref. Data*, 1981, **10**(1), 71–87.

38 L. Konermann, Addressing a common misconception: ammonium acetate as neutral pH 'buffer' for native electrospray mass spectroscopy, *J. Am. Soc. Mass Spectrom.*, 2017, **28**, 1827–1835.

39 Silver Fern Chemical Inc. Product description page: Ammonium Acetate Buffer (CAS No: 631-61-8). URL: http://www.silverfernchemical.com/products/ammonium-acetate-buffer/ [Accessed: 3rd May 2020].

40 R. M. Heck, R. J. Farrauto and S. T. Gulati, *Catalytic Air Pollution Control: commercial technology*, John Wiley & Sons, Inc., 3rd edn, 2009.

41 S. Plimpton, Fast Parallel Algorithms for Short-Range Molecular Dynamics, *J. Comput. Phys.*, 1995, **117**, 1–19.

42 W. C. Swope, H. C. Andersen, P. H. Berens and K. R. Wilson, A computer simulation method for the calculation of equilibrium constants for the formation of physical clusters of molecules: Application to small water clusters, *J. Chem. Phys.*, 1982, **76**, 637–649.

43 S. Nosé, A molecular dynamics method for simulations in the canonical ensemble, *Mol. Phys.*, 1984, **52**(2), 255–268.

44 W. G. Hoover, Canonical dynamics: equilibrium phase-space distributions, *Phys. Rev. A: At., Mol., Opt. Phys.*, 1985, **31**(3), 1695–1697.

45 R. W. Hockney and J. W. Eastwood, Chapter 8: Particle-Particle-Particle-Mesh (P3M) Algorithms, *Computer simulation using particles*, CRC Press, 1988, pp. 267–304, ISBN: 9780852743928.

46 H. J. C. Berendsen, J. R. Grigera and T. P. Straatsma, The missing term in effective pair potentials, *J. Phys. Chem.*, 1987, **91**(24), 6269–6271.

47 J. L. F. Abascal and C. Vega, A general purpose model for the condensed phases of water: TIP4P/2005, *J. Chem. Phys.*, 2005, **123**, 234505.

48 J. P. Ryckaert, G. Ciccotti and H. J. C. Berendsen, Numerical integration of the Cartesian equations of motion of a system with constraints: molecular dynamics of n-Alkanes, *J. Comput. Phys.*, 1977, **23**, 327–341.

49 I. S. Joung and T. E. Cheatham, Determination of alkali and halide monovalent ion parameters for use in explicitly solvated biomolecular simulations, *J. Phys. Chem. B*, 2008, **112**(30), 9020–9041.

50 H. Krienke and D. Opalka, Hydration of molecular ions: a molecular dynamics study with a SPC/E water model, *J. Phys. Chem. C*, 2007, **111**(43), 15935–15941.

51 S. Mamatkulov, M. Fyta and R. R. Netz, Force fields for divalent cations based on single-ion and ion-pair properties, *J. Chem. Phys.*, 2013, **138**, 024505.

52 S. Kashefolgheta and A. V. Verde, Developing force fields when experimental data is sparse: AMBER/GAFF-compatible parameters for inorganic and alkyl oxoanions, *Phys. Chem. Chem. Phys.*, 2017, **19**(31), 20593–20607.

53 W. D. Cornell, P. Cieplak, C. I. Bayly, I. R. Gould, K. M. Merz and D. M. Ferguson, *et al.*, *J. Am. Chem. Soc.*, 1995, **117**(19), 5179–5197.

54 J. Wang, R. M. Wolf, J. W. Caldwell, P. A. Kollman and D. A. Case, *J. Comput. Chem.*, 2004, **25**(9), 1157–1174.
55 J. Wang, P. Cieplak and P. A. Kollman, *J. Comput. Chem.*, 2000, **21**(12), 1049–1074.
56 W. L. Jorgensen and J. Tirado-Rives, *J. Am. Chem. Soc.*, 1988, **110**(6), 1657–1666.
57 D. J. Evans and G. P. Morriss, Nonlinear-response theory for steady planar Couette flow, *Phys. Rev. A: At., Mol., Opt. Phys.*, 1984, **30**(3), 1528–1530.
58 P. J. Daivis and B. D. Todd, A simple, direct derivation and proof of the validity of the SLLOD equations of motion for generalized homogeneous flows, *J. Chem. Phys.*, 2006, **124**, 194103.
59 B. Hess, Determining the shear viscosity of model liquids from molecular dynamics simulations, *J. Chem. Phys.*, 2002, **116**(1), 209–217.
60 A. Einstein, Über die von der molekularkinetischen Theorie der Wärme geforderte Bewegung von in ruhenden Flüssigkeiten suspendierten Teilchen, *Ann. Phys.*, 1905, **17**, 549–560. Available at: https://einstein-annalen.mpiwg-berlin.mpg.de/annalen/chronological/1905 (German), http://www.maths.usyd.edu.au/u/UG/SM/MATH3075/r/Einstein_1905.pdf (English; Dover Publications Inc., 1956). [Accessed: 4th May 2020].
61 E. Frey and K. Kroy, Brownian motion: a paradigm of soft matter and biological physics, *Ann. Phys.*, 2005, **14**(1–3), 20–50, DOI: 10.1002/andp.200410132.
62 G. Åkerlöf, A Study of the Composition of the Liquid Phase in Aqueous Systems containing Strong Electrolytes of Higher Valence Types as Solid Phases, *J. Phys. Chem.*, 1937, **41**(8), 1053–1076.
63 M. Aghaie, H. Aghaie and A. Ebrahimi, Thermodynamics of the solubility of barium nitrate in the mixed solvent, ethanol + water, and the related ion-association, *J. Mol. Liq.*, 2007, **135**(1–3), 72–74.
64 R. Wright, Selective Solvent Action. Part VI. The Effect of Temperature on the Solubilities of Semi-solutes in Aqueous Alcohol, *J. Chem. Soc.*, 1927, 1334–1337.
65 E. L. Hahn, Spin Echoes, *Phys. Rev.*, 1950, **80**(4), 580–594.
66 E. O. Stejskal and J. E. Tanner, Spin diffusion measurements: spin echoes in the presence of a time dependent field gradient, *J. Chem. Phys.*, 1965, **42**, 288–292.
67 M. Holz, S. R. Heil and A. Sacco, Temperature-dependent self-diffusion coefficients of water and six selected molecular liquids for calibration in accurate 1H NMRPFG measurements, *Phys. Chem. Chem. Phys.*, 2000, **2**(20), 4740–4742.
68 I. C. Yeh and G. J. Hummer, System-Size Dependence of Diffusion Coefficients and Viscosities from Molecular Dynamics Simulations with Periodic Boundary Conditions, *J. Phys. Chem. B*, 2004, **108**(40), 15873–15879.
69 J. S. Kim, Z. Wu, A. R. Morrow, A. Yethiraj and A. Yethiraj, Self-Diffusion and Viscosity in Electrolyte Solutions, *J. Phys. Chem. B*, 2012, **116**(39), 12007–12013.
70 M. Afzal, M. Saleem and M. T. Mahmood, Temperature and Concentration Dependence of Viscosity of Aqueous Electrolytes from 20 to 50 °C. Chlorides of Na^+, K^+, Mg^{2+}, Ca^{2+}, Ba^{2+}, Sr^{2+}, Co^{2+}, Ni^{2+}, Cu^{2+}, and Cr^{3+}, *J. Chem. Eng. Data*, 1989, **34**, 339–346.
71 H.-L. Zhang and S. J. Han, Viscosity and Density of Water + Sodium Chloride + Potassium Chloride Solutions at 298.15K, *J. Chem. Eng. Data*, 1996, **41**(3), 516–520.
72 A. A. Aleksandrov, E. V. Dzhuraeva and V. F. Utenkov, Viscosity of aqueous solutions of sodium chloride, *High Temp.*, 2012, **50**, 354–358.
73 J. Kestin, H. E. Khalifa and R. J. Correia, Tables of the dynamic and kinematic viscosity of aqueous NaCl solutions in the temperature range 20–150 °C and the pressure range 0.1–35 MPa, *J. Phys. Chem. Ref. Data*, 1981, **10**(1), 71. NIST weblink: https://srd.nist.gov/JPCRD/jpcrd176.pdf.
74 R. Fuentes-Azcatl and M. C. Barbosa, Sodium Chloride, NaCl/ε: New Force Field, *J. Phys. Chem. B*, 2016, **120**(9), 2460–2470.
75 D. W. McCall and D. C. Douglass, The effect of ions on the self-diffusion of water. I. Concentration dependence, *J. Phys. Chem.*, 1965, **69**(6), 2001–2011.
76 E. C. Meng and P. A. Kollman, Molecular Dynamics Studies of the Properties of Water around Simple Organic Solutes, *J. Phys. Chem.*, 1996, **100**(27), 11460–11470.
77 W. L. Jorgensen and J. Gao, Monte Carlo Simulations of the Hydration of Ammonium and Carboxylate Ions, *J. Phys. Chem.*, 1986, **90**(10), 2174–2182.
78 M. Ekimova, W. Quevedo, L. Szyc and M. Iannuzzi, *et al.*, Aqueous Solvation of Ammonia and Ammonium: Probing Hydrogen Bond Motifs with FT-IR and Soft X-ray Spectroscopy, *J. Am. Chem. Soc.*, 2017, **139**(36), 12773–12783.
79 S. Joung, T. Luchko and D. A. Case, Simple electrolyte solutions: Comparison of DRISM and molecular dynamics results for alkali halide solutions, *J. Chem. Phys.*, 2013, **138**(4), 044103.
80 P. Banerjee, S. Yashonath and B. Bagchi, Coupled jump rotational dynamics in aqueous nitrate solutions, *J. Chem. Phys.*, 2016, **145**(23), 234502.
81 R. Caminiti, G. Licheri, G. Piccaluga and G. Pinna, On NO^-_3–H_2O interactions in aqueous solutions, *J. Chem. Phys.*, 1978, **68**(4), 1967–1970.
82 A. L. Thompson, D. Parker, D. A. Fulton and J. A. K. Howard, *et al.*, On the role of the counter-ion in defining water structure and dynamics: order, structure and dynamics in hydrophilic and hydrophobic gadolinium salt complexes, *Dalton Trans.*, 2006, 5605–5616.
83 P. Naert, K. Rabaey and C. V. Stevens, Ionic liquid ion exchange: exclusion from strong interactions condemns cations to the most weakly interacting anions and dictates reaction equilibrium, *Green Chem.*, 2018, **20**, 4277–4286.
84 H. Luo, S. Dai, P. V. Bonnesen, T. J. Haverlock, B. A. Moyer and A. C. Buchanan III, A Striking Effect of Ionic-Liquid Anions in the Extraction of Sr2+ and Cs+ by Dicyclohexano-18-Crown-6, *Solvent Extr. Ion Exch.*, 2006, **24**(1), 19–31.
85 S. Sankarasubramanian, J. Kahky and V. Ramani, Tuning anion solvation energetics enhances potassium-oxygen battery performance, *Proc. Natl. Acad. Sci. U. S. A.*, 2019, **116**(30), 14899–14904.

86 P. Banerjee and B. Bagchi, Rotational dynamics of polyatomic ions in aqueous solutions: from continuum model to mode-coupling theory, aided by computer simulations, *J. Chem. Phys.*, 2018, **148**, 224504.
87 Y. Marcus, Thermodynamics of solvation of ions. Part 5. Gibbs free energy of hydration at 298.15K, *J. Chem. Soc., Faraday Trans.*, 1991, **87**(18), 2995–2999.
88 M. I. Chaudhari, M. Soniat and S. B. Rempe, Octacoordination and the aqueous Ba^{2+} ion, *J. Phys. Chem. B*, 2015, **119**(28), 8746–8753.
89 F. Aydin, C. Zhan, C. Ritt, R. Epsztein, M. Elimelech, E. Schwegler and T. A. Pham, Similarities and differences between potassium and ammonium ions in liquid water: a first principles study, *Phys. Chem. Chem. Phys.*, 2020, **22**, 2540–2548.
90 S. Varma and S. B. Rempe, Coordination numbers of alkali metal ions in aqueous solutions, *Biophys. Chem.*, 2006, **124**, 192–199.
91 A. Tongraar, P. Tangkawanwanit and B. M. Rode, A combined QM/MM molecular dynamics simulations study of nitrate anion (NO_3^-) in aqueous solution, *J. Phys. Chem. A*, 2006, **110**, 12918–12926.
92 M. V. Fedotova and S. E. Kruchinin, Hydration of acetic acid and acetate ion in water studied by 1D-RISM theory, *J. Mol. Liq.*, 2011, **164**, 201–206.
93 R. Mancinelli, A. Botti, F. Bruni, M. A. Ricci and A. K. Soper, Hydration of sodium, potassium and chloride ions in solution and the concept of structure maker/breaker, *J. Phys. Chem. B*, 2007, **111**(48), 13570–13577.
94 PubChem (https://pubchem.ncbi.nlm.nih.gov/): compound summary webpages for 'barium', 'ammonium', 'sodium', 'nitrate', 'acetate' and 'chloride' - Section 3.1, Computed Properties, [Accessed: 9th July 2020].
95 W. M. Haynes, D. R. Lide and T. J. Bruno, *CRC Handbook of Chemistry and Physics*, Section 5-66: Thermodynamic properties of aqueous ions, CRC Press, 95th edn, 2014–2015.
96 J. B. Hendrickson, P. Huang and A. G. Toczko, Molecular Complexity – A Simplified Formula Adapted to Individual Atoms, *J. Chem. Inf. Comput. Sci.*, 1987, **27**, 63–67; W. D. Ihlenfeldt, Computergestützte Syntheseplanung durch Erkennung synthetisch nutzbarer Möglichkeit von Molekülen, PhD thesis, TU Munich, 1991.
97 A. Zuber, R. F. Checoni, R. Mathew, J. P. L. Santos, F. W. Tavares and M. Castier, Thermodynamic properties of 1:1 salt aqueous solutions with the electrolattice equation of state, *Oil Gas Sci. Technol.*, 2013, **68**(2), 255–270.
98 K. D. Collins, Charge density-dependent strength of hydration and biological structure, *Biophys. J.*, 1997, **72**(1), 65–76.
99 S. D. Deosarkar and M. S. Mendkudle, Physicochemical properties and Ion-Solvent interactions in aqueous sodium, ammonium and lead acetate solution, *Russ. J. Phys. Chem. A*, 2014, **88**(9), 1527–1532.
100 T. H. Doan and J. Sangster, Viscosities of concentrated aqueous solutions of some 1:1, 2:1 and 3:1 nitrates at 25 °C, *J. Chem. Eng. Data*, 1981, **26**(2), 141–144.
101 J. Padova, Ion-Solvent Interaction in Mixed Solvents. II. The Viscosity of Electrolytes in Mixed Solvents, *J. Chem. Phys.*, 1963, **38**(11), 2635–2640.